Polymer 50 (2009) 6129–6138

Contents lists available at ScienceDirect

Polymer

journal homepage: www.elsevier.com/locate/polymer

Effects of block length and solution-casting conditions on the final morphology and properties of disulfonated poly(arylene ether sulfone) multiblock copolymer films for proton exchange membranes

Myoungbae Lee [a], Jong Keun Park [b], Hae-Seung Lee [b], Ozma Lane [b], Robert B. Moore [b], James E. McGrath [b], Donald G. Baird [a,*]

[a] Department of Chemical Engineering, Virginia Tech, Blacksburg, VA 24061, USA
[b] Macromolecules and Interfaces Institute, Virginia Tech, Blacksburg, VA 24061, USA

ARTICLE INFO

Article history:
Received 31 July 2009
Received in revised form
6 October 2009
Accepted 9 October 2009
Available online 4 November 2009

Keywords:
Proton exchange membrane
Multiblock copolymer
Effects of solution-casting conditions

ABSTRACT

The effects of block length and solution-casting conditions on the final microstructures and properties of disulfonated poly(arylene ether sulfone) multiblock copolymer (BPSH100–BPS0) films for proton exchange membranes were investigated based on the basic principles of microstructure formation of block copolymers. Morphological studies using transmission electron microscopy and small angle X-ray scattering demonstrated that as the block length increased, the inter-ionic-domain distance increased, with a subsequent increase in lamellar ordering and long-range continuity. Further enhancement in morphological order was achieved by simply utilizing a selective solvent, dimethylacetamide, which is good and marginal for the sulfonated and unsulfonated blocks, respectively, rather than a neutral solvent, *N*-metyl-2-pyrrolidone. These morphological enhancements led to higher proton conductivity and water uptake. Drying temperature and/or solvent removal rate were observed to have considerable effects on water uptake and swelling behavior, being coupled with solvent selectivity. Also, the multiblock copolymer consisting of longer blocks was found to be more sensitive to the variation of the processing conditions such as solvent type and film drying temperature.

© 2009 Elsevier Ltd. All rights reserved.

1. Introduction

Proton exchange membrane (PEM) fuel cell (FC) has been proposed as an alternative energy conversion technology due to its high efficiency and environment-friendly nature [1]. However, its widespread commercialization is far from being fulfilled because of a number of technical problems remaining to be solved. Currently, insufficient performance of PEMs at elevated temperatures and low humidity, platinum catalysts that are susceptible to carbon monoxide, and cost are some of the main issues [2]. In order for fuel cells to be widely used, significant scientific and technological progress is needed as well as considerable cost reduction. In particular, operation of the fuel cell at elevated temperatures above 120 °C is highly desirable [3]. Elevated temperature operations not only increase the reaction rates at the electrodes but also enable reduction of carbon monoxide poisoning of the platinum catalyst and even potential utilization of more economical catalysts.

Nafion has been a benchmark PEM material for years owing to its outstanding properties such as excellent proton conductivity under certain conditions, endurance in the fuel cell environment, mechanical toughness and moderate water uptake [4,5]. However, it is generally recognized that perfluorinated Nafion-type membranes are inappropriate for elevated temperature operation [6]. Absorbed water in the membranes lowers the glass transition temperature, which leads to deterioration of mechanical properties and fuel cell performance as well [7,8]. In addition, high cost and high permeability to methanol are major drawbacks of the Nafion-type membranes.

Over the last decade, researchers have tried to produce PEMs with improved performance by employing promising materials [9]. Numerous materials and their variations based on hydrocarbons such as polyaromatic or polyheterocyclic repeat units have been introduced as alternative PEM materials due to their excellent thermal, oxidative and hydrolytic stability, good mechanical properties, and availability. Partially sulfonated random copolymers based on the hydrocarbon-based candidate materials were obtained via direct copolymerization or post-sulfonation, and their performances and properties for PEM applications were examined [5]. The proton conductivities under fully hydrated conditions and excellent

* Corresponding author. Tel.: +1 540 231 5998; fax: +1 540 231 2732.
E-mail address: dbaird@vt.edu (D.G. Baird).

0032-3861/$ – see front matter © 2009 Elsevier Ltd. All rights reserved.
doi:10.1016/j.polymer.2009.10.023

stability indicated that the partially sulfonated random copolymers were promising as PEMs. However, their proton conductivities at low humidity were significantly lower than the Nafion-type membranes (~0.1 S/cm at 80 °C and 50% relative humidity).

More recently, extensive efforts are being devoted to improve the performance of the hydrocarbon-based PEMs at low humidity by modifying their molecular architecture. It has been demonstrated that the microstructure of PEMs is crucial for their performance in the operation of fuel cells [10]. As the continuity and ion-richness of the sulfonated hydrophilic domains increased, PEMs showed improved performance. Several previous studies hypothesized that block copolymer PEMs consisting of sulfonated and unsulfonated blocks would result in the formation of more continuous and ion-rich hydrophilic domains and, accordingly, improved performance of PEMs [11–16], because block copolymer systems can develop phase-separated ordered microstructures such as lamellae, gyroid, and cylinders [17]. Sulfonated block copolymers based on the poly-aromatic or polyheterocyclic repeat units have been introduced and evaluated as PEMs. Their results showed that the proton conductivities of the block copolymer PEMs were noticeably higher than those of the random copolymer PEMs in spite of similar degrees of sulfonation. Lee et al. [13] also showed that the PEMs consisting of longer blocks of disulfonated poly(arylene ether sulfone) (PAES) and unsulfonated polyimide produced higher proton conductivity due to more continuous hydrophilic domains based on their morphological study using atomic force microscopy.

For the evaluation of new PEM materials at the early stage of their development, membranes are usually prepared based on a lab-scale batch casting method: dilute polymer solutions are cast onto glass plates through syringe-filters, with the solvent then being removed by means of evaporation using an oven or a heat lamp. The casting process is critical for a successful production of polymeric thin membranes because it has substantial influences on the microstructure and properties [18]. Thus, it is essential to identify the effects of processing conditions and to utilize an appropriate processing technique.

In several previous studies the importance of PEM processing conditions has been reported. Recently, Bébin and Galiano [19,20] examined the possibility of using melt-extrusion for the manufacture of partially sulfonated PEEK random copolymer PEMs with the help of suitable plasticizers. They observed that the melt-cast PEMs exhibited proton conductivity values that were one half of those of the solution-cast PEMs. Even though these previous studies strongly implied that processing conditions have substantial effects on the final properties of PEMs, the significance of material processing have not gained much attention so far. Large discrepancies in proton conductivity data among PEMs with similar composition presented in previous studies could be due to different processing conditions, as already pointed out by Robertson et al. [21].

In the case of block copolymer PEMs, processing conditions are anticipated to play a more dominant role in the formation of final morphology and, accordingly, final properties because of the basic principles for microstructure formation of block copolymers. However, the principles have been underestimated in the processing of block copolymer PEMs despite the general recognition of the fact that the aforementioned hydrocarbon-based PEM materials are a typical type of block copolymers consisting of two distinct blocks (e.g., sulfonated and unsulfonated ones). Recently, Huang et al. [22] reported that the proton conductivity of a block copolymer significantly depended on drying conditions, possibly such as drying temperature, initial solution concentration, and solvent removal rate, while they were exploring the possibility of manufacturing the PEM films by solvent-casting using a reverse-roll coating technique.

A variety of microstructures of block copolymers can be induced by microphase separation due to the phase behavior of block copolymers [17]. Khandpur et al. [23] represented the phase behavior of styrene-isoprene (SI) diblock copolymers as a function of two parameters, $\chi_{AB}N$ and f. Here, χ_{AB} is the Flory–Huggins interaction parameter, which indicates the dissimilarity between different component blocks (A and B). N is the degree of polymerization, which is the number of statistical segments per chain, and f is the volume fraction of one component block. According to the diagram, when the product $\chi_{AB}N$ is larger than a critical value, $(\chi_{AB}N)_{ODT}$ (ODT = order-disorder transition), for a certain value of f, phase separation of the block copolymer occurs and a periodically ordered structure such as lamellae, gyroid, etc. develops on a microscale of approximately 5–500 nm. That is, once a block copolymer is synthesized, N and f are no longer variable, but χ_{AB} can still be adjustable during processing because χ_{AB} is inversely proportional to temperature, i.e., $\chi_{AB} = C_1 + C_2/T$. Additionally, in a solution, the phase behavior of diblock copolymers is controlled by the interactions between the solvent and the two component blocks ($\chi_{solv\text{-}A} = C_3 + C_4/T$ and $\chi_{solv\text{-}B} = C_5 + C_6/T$) as well as the interaction between the two component blocks (χ_{AB}) [24]. These basic principles strongly imply that the processing temperature and solvent selectivity are vital processing conditions of block copolymers for PEMs. Hanley et al. [25] generated the phase diagrams of a styrene-isoprene (SI) diblock copolymer as a function of temperature and volume fraction in four different solvents with different degrees of selectivity. They observed that the phase of a block copolymer significantly depended on solvent selectivity and temperature. It can also be observed that the SI diblock copolymer in a more selective solvent had a greater tendency to form ordered structures.

Additionally, Huang et al. [26] showed that the kinetics of phase separation of block copolymers was one of the crucial factors that decided the final morphology of solution-cast block copolymer films. They obtained different microstructures from solution-cast styrene-butadiene-styrene triblock and styrene-butadiene diblock copolymer films by varying the rate of solvent evaporation at room temperature (~25 °C). Normal equilibrium cylindrical or spherical microstructures with polystyrene cylinders or spheres in polybutadiene matrices were observed from the films dried for a prolonged time by suppressing the rate of solvent evaporation in a partially solvent-saturated environment. However, drying of the films for an abridged time in a less solvent-saturated environment resulted in "kinetically frozen-in" inverted cylindrical or spherical microstructures, where polybutadiene cylinders or spheres were embedded in polystyrene matrices, because the polymer molecules had insufficient time to rearrange to the equilibrium microstructures.

Therefore, the primary objective of this study is to initially investigate the effects of solvent selectivity, drying temperature, and solvent removal rate on the final microstructure and properties of PEMs from the viewpoint of microphase separation of block copolymers. For this study a statistically random PAES copolymer with 35 mol% disulfonation (BPSH35) as a control and three multi-block copolymers consisting of wholly disulfonated and unsulfonated PAES blocks (BPSH100 and BPS0, respectively) with three different lengths (for chemical structures, see Fig. 1), which have proven to be promising PEM materials as reported in previous works [11,27], were prepared and utilized. In order to assess the morphology developed during film drying, transmission electron microscopy (TEM) and small angle X-ray scattering (SAXS) were used.

2. Experimental

2.1. Synthesis and characterization of copolymers

BPSH35 random copolymer was synthesized by potassium carbonate mediated direct aromatic nucleophilic substitution

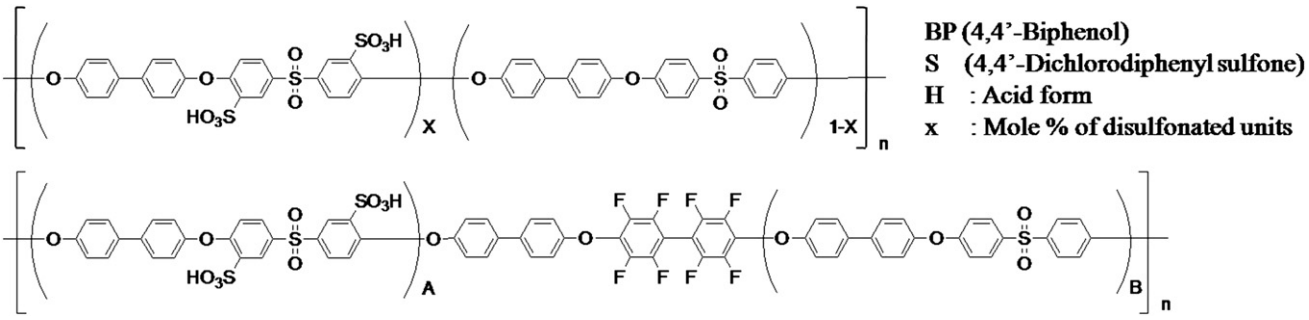

Fig. 1. Chemical structures of BPSH35 random (top) and BPSH100–BPS0 multiblock (bottom) copolymer.

polycondensation of disodium 3,3′-disulfonate-4,4′-dichlorodiphenylsulfone, 4,4′-dichlorodiphenylsulfone and 4,4′-biphenol as introduced by Wang et al. [27]. BPSH100–BPS0 multiblock copolymers were prepared by a coupling reaction between phenoxide terminated disulfonated PAES (BPSH100) and decafluorobiphenyl end-capped unsulfonated PAES (BPS0) oligomers with the block lengths of 5, 10, and 15 kg/mol. Details on the synthesis of the oligomers and multiblock copolymers can be found elsewhere [11]. Intrinsic viscosities (IV) were determined in *N*-methyl-2-pyrrolidone (NMP) containing 0.05 M LiBr at 25 °C using an Ubbelohde viscometer and the ion-exchange capacity (IEC = moles SO_3^- per gram sample) values were determined by titration with a standard NaOH solution. The measured values of IVs and IECs are presented in Table 1. The IV values were sufficiently high so that tough and ductile membranes could be produced. Compared with the BPSH35 random copolymer, the IEC values of the multiblock copolymers were slightly lower, but they were close to each other, ranging from 1.34 to 1.40 meq/g. The multiblock copolymers with similar IEC values were obtained by using 1:1 stoichiometry between the BPSH100 and BPS0 blocks with equal block lengths.

2.2. Membrane preparation

The copolymers in their salt form were dissolved in NMP or dimethylacetamide (DMAC) (Sigma, ≥99%, used as received) (15 w/v%) by stirring at 60 °C overnight. The solutions were filtered using 5 μm Teflon® syringe-filters. Then about 250 μm thick wet films with an area of 3.5 cm × 8 cm were cast onto clean stainless steel substrates using a hand-casting knife. The wet films were dried using the batch convection drying apparatus described below in detail. The velocity of the convection air was maintained at 0.2 m/s. The temperature of the convection air was varied between room temperature (~20 °C) and 80 °C. Room temperature was the lowest temperature available without any supplementary equipment and 80 °C was the critical temperature, above which bubbling defects significantly occurred because of the high vapor pressure of the solvents. The temperature variation of the convection air above the wet films was less than ±2 °C during the drying process. The films were additionally dried overnight at 110 °C *in vacuo* to remove the residual solvent. Finally, about 25 μm thick dry films were obtained. The resultant films were acidified by immersing in 0.5 M boiling sulfuric acid aqueous solution for 2 h. To remove residual sulfuric acid in the films, the acidified films were immersed in boiling deionized (DI) water for 2 h.

Table 1
Copolymer characteristics.

Copolymer	IV [dL/g]	IEC [meq/g]
BPSH35	0.74	1.51
BPSH100–BPS0 (5–5 k)	1.01	1.39
BPSH100–BPS0 (10–10 k)	0.89	1.34
BPSH100–BPS0 (15–15 k)	0.94	1.40

2.3. Batch convection drying apparatus

Typically forced convection is used as a primary drying method in industry because of its advantages (e.g., faster drying rate) over conduction and radiation [28]. Convection air not only supplies the energy necessary for solvent evaporation but also facilitates the mass transport at the air–liquid interface by sweeping away solvent vapor. Thus, to generate film drying conditions at a semi-industrial level in the laboratory, a batch convection drying apparatus was designed and built by adopting the device used by previous studies [29]. A schematic of the apparatus is presented in Fig. 2. A flowmeter and two air heaters were employed for the control of air velocity and temperature, respectively. The convection air passed through a rectangular aluminum duct. A stainless steel substrate was placed on a metal shaft connected to a balance through a passage on the bottom of the duct. A computer connected to the balance through an interface enabled recording the change in the weight of the wet films during the drying process and, consequently, calculation of drying rate and total drying time. A detachable glass window positioned right above the substrate allowed introduction of samples and visual observation during film drying.

2.4. Proton conductivity measurement

Proton conductivity of the membrane was measured using a Solatron (1252A + 1287) Impedance/Gain-Phase Analyzer over the frequency range of 10 Hz–1 MHz. The resistance of the membrane was measured at the frequency that generated the minimum imaginary response using the cell devised by Zawodzinski et al. [30]. Then proton conductivity of the membrane was determined from the resistance, the dimensions of the cell, and thickness of the membrane. For measurement of proton conductivity at 30 °C and under fully hydrated conditions, membranes were equilibrated in DI water for 24 h.

2.5. Water uptake measurement

Water uptake is the ratio of the weight of water absorbed by the membrane to the weight of the dry membrane. Water uptake was determined by measuring the weight of the sample in dry and wet states (W_{dry} and W_{wet}, respectively) and, then, by use of the following equation:

$$\text{Water uptake} = \frac{W_{wet} - W_{dry}}{W_{dry}} \times 100\ (\%) \quad (1)$$

For the measurement of W_{wet}, the sample was immersed in DI water for 24 h at room temperature, blotted dry, and then weighed.

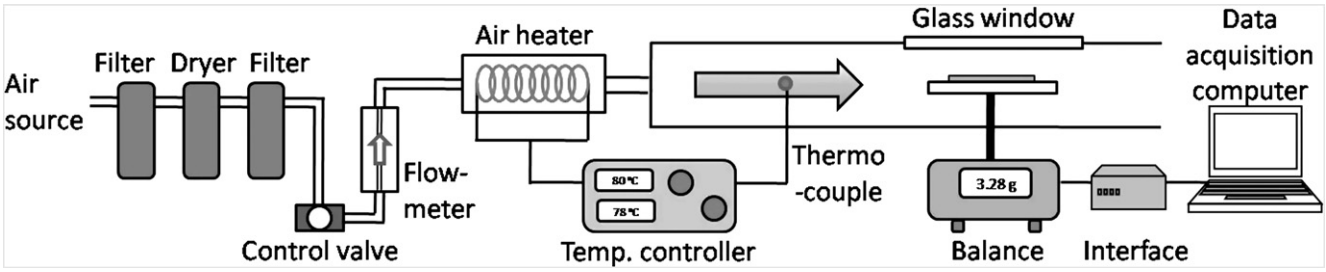

Fig. 2. Schematic of batch convection drying apparatus.

The dry wet, W_{dry}, was measured for samples dried in a vacuum oven at 120 °C for 30 min before weighing.

2.6. Determination of swelling ratio

The swelling ratios of membranes were determined by measuring the in-plane dimensions (x and y) and through-plane dimension (z) of the dry and wet membranes using a vernier caliper and a thickness gauge with 1 μ resolution, respectively. The dry and wet membranes were prepared in the same method as for the water uptake measurement.

Based on the wet membrane dimensions, the ion-exchange capacity of the hydrated membranes was also calculated on a volumetric basis, IEC_v as the moles SO_3^- per volume of sample. For membranes of known dry weight, the volumetric ion-exchange capacity was calculated as: $IEC_v = IEC(W_{dry}/V_{wet})$.

2.7. Transmission electron microscopy

The hydrogen ions were replaced with cesium ions by immersing the membrane samples in an aqueous solution with excessive amount of CsOH, which resulted in appropriate enhancement of electron density contrast. Then samples were embedded in epoxy and ultra-microtomed into about 100 nm thick pieces with a diamond knife. Transmission electron micrographs were attained by operating a Philips EM 420 Transmission Electron Microscope at an accelerating voltage of 100 kV.

2.8. Synchrotron small angle X-ray scattering

SAXS profiles were acquired at the Brookhaven National Laboratory on the Advanced Polymer Beamline (X27C) at the National Synchrotron Light Source. Due to the lack of electron density differences between the ionic and non-ionic domains of the copolymers in their acid form, all the samples were neutralized to contain Cs^+ ions as with TEM experiments. The wavelength of the X-ray beam was 1.366 Å and the sample-to-detector distance 1904.67 mm. Two-dimensional SAXS images were recorded using a Mar CCD camera with an intensity uncertainty on the order of 2% and analyzed using the POLAR software developed by Stonybrook Technology and Applied Research, Inc. All scattering intensities were corrected for transmission and background scatter due to air and Kapton windows and represented in arbitrary, relative intensity units as a function of the scattering vector, q, which is a function of the scattering angle through the following relationship, $q = (4\pi/\lambda) \sin\theta$, where λ is the wavelength of X-ray beam (1.366 Å) and θ is half of the scattering angle (2θ).

3. Results and discussion

Acronyms for the multiblock copolymer films will be used for convenience, henceforth, where '5 k NMP film' implies the BPSH100–BPS0 (5–5 k) multiblock copolymer film cast with NMP.

3.1. Film-casting and -drying

The characteristic drying curves of the 15 k films are presented in Fig. 3 as remaining amount of solvent vs. drying time. The drying curves showed a traditional film drying behavior. Initially, the drying rates remained almost constant as long as the rate of the solvent diffusion through the wet film was comparable with the rate of solvent evaporation at the surface of the wet films [28]. As the drying of the wet film proceeded, the concentration of the copolymer in the wet film increased and the diffusive transfer of solvent molecules was limited by the polymer molecules. Hence, the film drying became controlled by diffusion of the solvent through the polymer film and the drying rate gradually decreased.

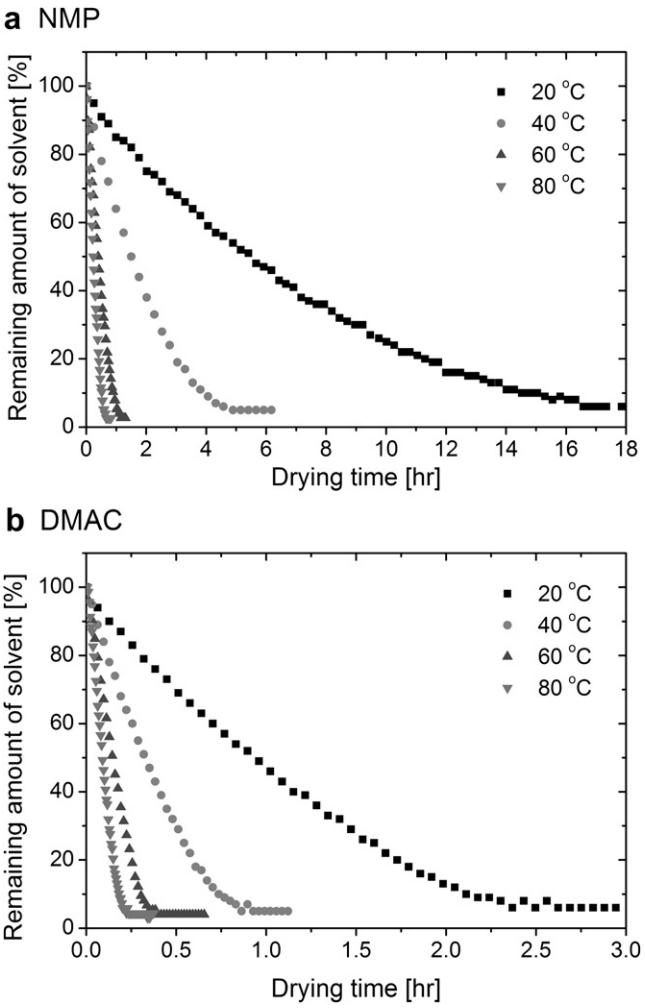

Fig. 3. Characteristic film drying curves as a function of temperature of convection air at 0.2 m/s.

Table 2
Comparison of total drying time between NMP and DMAC films.

Convection air temp. [°C]	Total drying time [h]	
	NMP	DMAC
20	16.5	2.4
40	4.9	0.9
60	1.2	0.4
80	0.7	0.2

As expected, the drying rate and total drying time significantly depended on the solvent type and convection air temperature. The total drying time of the 15 k films is summarized in Table 2. For this estimation, time required to remove the residual solvent using a vacuum oven was not considered. Drying of the films cast with DMAC proceeded faster due to the higher vapor pressure of DMAC. For example, at 60 °C, the vapor pressure of DMAC (11.0 mm Hg) is about three times as high as that of NMP (3.7 mm Hg) [31]. Thus, drying of the 15 k DMAC film was completed in one-third of the total drying time of the 15 k NMP film. Likewise, film drying at a higher temperature considerably accelerated the drying process due to the elevated vapor pressure. The total drying time at 20 °C was longer than at 80 °C by more than an order of magnitude.

3.2. Determination of solvent selectivity

The degrees of solvent selectivity of NMP and DMAC for the component blocks were determined by measuring the solubility of the wholly sulfonated BPSH100 (15 k) and unsulfonated BPS0 (15 k) oligomers in each solvent. At room temperature (~20 °C), more than 30 g of the BPSH100 oligomer was readily dissolved in 100 ml of both NNP and DMAC. However, the solubility of the BPS0 oligomer was about 9 g in 100 ml of DMAC, while more than 30 g of the BPS0 oligomer was dissolved in NMP. That is, both NMP and DMAC are good solvents for the sulfonated BPSH100 oligomer but good and marginal, respectively, for the unsulfonated BPS0 oligomer at room temperature ($\chi_{BPS0\text{–}DMAC} > \chi_{BPS0\text{–}NMP}$). However, at 80 °C, DMAC was also a good solvent for the BPS0 oligomer so that more than 30 g of the BPS0 oligomer was dissolved in 100 ml of DMAC ($\chi_{BPS0\text{–}DMAC} = f(T)$).

3.3. Properties of PEMs

The resultant films were evaluated as PEMs by measuring the proton conductivity, water uptake, and swelling behavior in order to investigate the effects of solvent selectivity and film drying conditions as well as the block length of the multiblock copolymers.

Fig. 4 presents the proton conductivities of the BPSH100–BPS0 multiblock copolymer films measured at 30 °C under fully hydrated conditions. It is obvious that the block copolymer system was more advantageous for proton conduction over the random copolymer, as already reported elsewhere [11]. The proton conductivities of the multiblock copolymer films were comparable or higher than that of the BPSH35 random copolymer film despite the slightly lower IEC values. Also, the proton conductivity increased with increasing block length. The proton conductivities of the 15 k films were significantly higher than those of the 5 k films, while the 10 k films showed a slight increase compared to the 5 k films. Solvent selectivity also turned out to be a crucial factor for the proton conductivities of the multiblock copolymer films. The proton conductivities of the multiblock copolymer films were considerably increased by simply using DMAC as a casting solvent, which is selective for the BPSH100 block, instead of NMP, a good solvent for both BPSH100 and BPS0 blocks. In the case of the 15 k films, the proton conductivities of the DMAC films were higher than those of the NMP films by almost 50%.

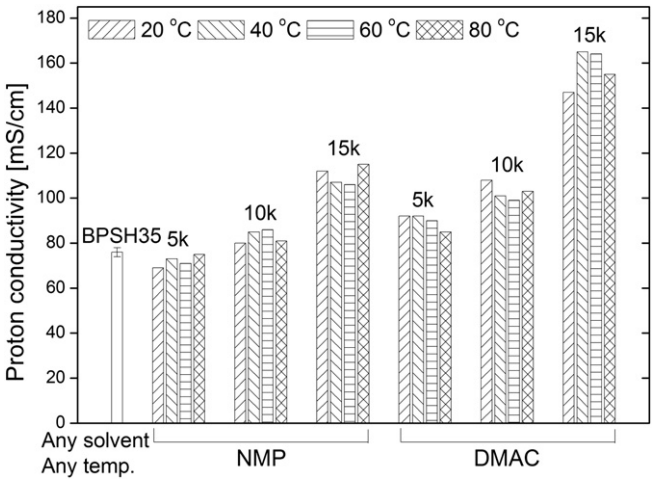

Fig. 4. Effects of block length and solvent type on proton conductivity of the BPSH100–BPS0 multiblock copolymer films (measured at 30 °C and fully hydrated conditions).

Just as observed from the proton conductivity, significant effects of block length and solvent selectivity on the water uptake of the multiblock copolymer films were observed. Fig. 5 represents the water uptake measurement results of the multiblock copolymer films. The water uptake also increased with increasing block length and utilization of DMAC also increased the water uptake of the multiblock copolymer films by the magnitudes comparable to the effects on the proton conductivity. However, it is noteworthy that the drying temperature had substantial effects on the water uptake, although no obvious effects of drying temperature were observed from the proton conductivity. Drying of the multiblock copolymer films at a lower temperature induced higher water uptake. All the DMAC films and 15 k NMP films showed this trend, while the water uptake of the 5 k and 10 k NMP films still did not show obvious dependence on the drying temperature. The effect of drying temperature was most severe for the 15 k DMAC films; drying at 20 °C caused more than twice the increase in the water uptake of the film, compared with drying at 80 °C. In general, the proton conductivity increased with increasing water uptake, because both proton conductivity and water uptake depend on the ion contents and degree of aggregation [27,32]. However, this result is not in agreement with the proton conductivity result, which showed no significant dependence on the drying temperature. The 15 k DMAC films dried at 20 and 80 °C produced comparable proton conductivities despite the huge difference in their water uptake.

This discrepancy can be explained by investigating the swelling behavior of the multiblock copolymer films. The swelling behavior of the 15 k DMAC films, of which water uptake showed the highest degree of dependence on the drying temperature, is presented in Fig. 6. As opposed to the BPSH35 random copolymer films, the 15 k DMAC films showed an anisotropic swelling behavior. The through-plane swelling of the 15 k DMAC films was much larger than the in-plane swelling. This anisotropic swelling behavior of the 15 k DMAC films may be a macroscopic indication of ordered microstructures of the multiblock copolymer films [11]. As well, it is clearly shown that the through-plane swelling of the 15 k DMAC films significantly depended on the drying temperature, while the in-plane swelling showed no obvious dependence. Drying of the film at a lower temperature significantly increased the through-plane swelling. The through-plane swelling of the 15 k DMAC film dried at 20 °C was larger than that of the 15 k DMAC film dried at 80 °C to the extent comparable to the increase in the water uptake. Definitely, this difference in the swelling of the multiblock copolymer films led to the difference in the volume of the films in

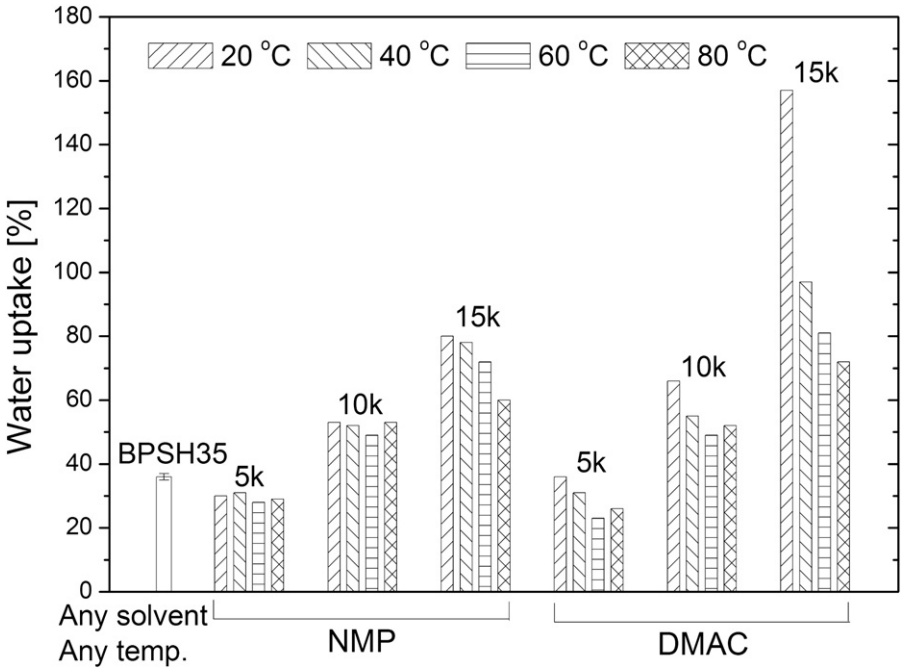

Fig. 5. Effects of block length and casting conditions on water uptake of the BPSH100–BPS0 multiblock copolymer films (measured at 20 °C).

a wet state and, consequently, in the number of proton-conducting moieties per unit volume of the wet films, IEC_v. These IEC_v measurements were conducted for the 4 multiblock copolymers, which showed a dependence of water uptake on the drying temperature (5, 10, and 15 k DMAC films and 15 k NMP films). Fig. 7 displays the estimated volume-based IEC_v values of the wet multiblock copolymer films dried at different temperatures. Generally, the multiblock copolymer films dried at lower temperatures had lower volume-based IEC_v values. Moreover, as the block length increased, the trend of increasing IEC_v with drying temperature became more pronounced. Because the data in Figs. 4 and 5 clearly show a disconnect between conductivity and water uptake, the discrepancy may be explained by consideration of the IEC_v, which effectively accounts for dilution of proton-conducting sites [33]. For example, the water uptake of the 15 k DMAC films varied strongly with drying temperature, resulting in a significant dilution of the proton-conducting sites with decreasing casting temperature. Because the proton conductivity for this series of samples remained relatively constant, it is reasonable to conclude that this dilution phenomenon is responsible for the unexpected independence of proton conductivity on drying temperature.

It is of interest to note that the volume-based IEC_v values of the multiblock copolymers, except the 5 k films, were significantly lower than that of the BPSH35 random copolymer; however, the multiblock copolymer films produced significantly higher proton conductivities. Furthermore, the data in Fig. 4 clearly show proton conductivity increases with block length. Even with lower or similar volume-based IEC_v values, the proton conductivities of the 15 k films were considerably higher than any of the other copolymer films studied here. Based on this observation, it is apparent that the block copolymer system facilitates the effective utilization of proton-conducting moieties. This phenomenon is likely linked to the unique morphology of these block copolymer systems, as discussed below.

It can also be concluded that the unique architecture of the multiblock copolymers consisting of longer block lengths is

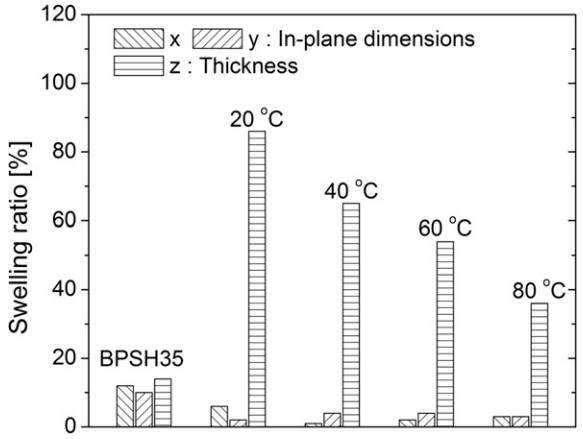

Fig. 6. Swelling behavior of the BPSH100–BPS0 (15–15 k) copolymer films cast with DMAC as a function of drying temperature.

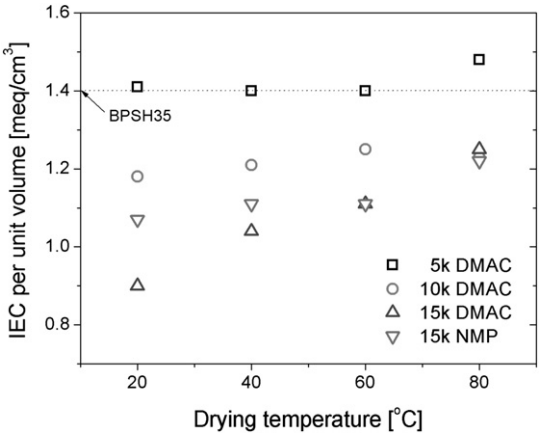

Fig. 7. Estimated volume-based IEC_v values of the multiblock copolymer films in a wet state.

responsible for properties that are more responsive to variations in the processing conditions from the following observations. In the first place, the magnitude of the solvent selectivity effects on proton conductivity and water uptake of the 15 k films was greater than that of the 5 k and 10 k films. For example, the utilization of DMAC increased the proton conductivity of the 15 k film by almost 50%, while only a 20–25% increase was observed for that of the 5 k and 10 k films. Secondly, the effects of the drying temperature on the water uptake of the 15 k DMAC films were significant, but the water uptake of the 5 k and 10 k DMAC films showed only a mild dependence on the drying temperature. Lastly, the water uptake of only the 15 k NMP films varied with the drying temperature, while the water uptake of the 5 k and 10 k NMP films showed no dependence on the drying temperature. In contrast to the responsive behavior of the multiblock copolymers, it is important to note that the properties of the BPSH35 random copolymer films were essentially independent of processing conditions. Because the proton-conducting groups in the random copolymer are more homogeneously distributed along the chains, relative to the multiblocks, this observation further supports the importance of chain architecture on the ability to control properties by variations in processing conditions.

3.4. Morphology of PEMs

A morphological study was conducted using TEM and synchrotron SAXS to identify the microstructures of the BPSH35 random copolymer and the BPSH100–BPS0 multiblock copolymer films and to investigate the effects of casting conditions on the resulting microstructures. The TEM micrographs of the copolymer films cast with NMP and dried at 20 °C are presented in Fig. 8. The unsulfonated BPS0 block domains appear brighter in the micrographs, while the sulfonated BPSH100 block domains appear darker due to the presence of electron-rich ion-pairs obtained by cesium neutralization. As shown in Fig. 8(a), the BPSH35 random copolymer film produced a featureless image indicating the absence of well-defined ionic domains and a relatively homogeneous distribution of ionic groups within the polymer matrix. Because the ions in BPSH35 are randomly (i.e., homogeneously) distributed along the polymer chains, this lack of large-scale morphological order is consistent with the statistical chain structure. In contrast, the multiblock copolymer films (Fig. 8(b)∼(d)) showed well-defined ionic domains indicating large-scale phase separation between the sulfonated and unsulfonated blocks. These TEM micrographs also showed the effects of the block length on the order of the domain microstructure. As the block length increased from 5 to 15 kg/mol, the multiblock copolymer films developed a more coarsely phase-separated morphology with longer-range continuity and wider inter-domain spacings. As discussed earlier, the proton conductivity and water uptake increased with increasing block length. Thus, it is reasonable to attribute the increased proton conductivity and water uptake to the effects of block length on the formation of more continuous and wider ionic domains.

The SAXS profiles of the BPSH100–BPS0 multiblock copolymer films cast with NMP and dried at 20 °C are presented in Fig. 9. In the investigated range of scattering wave vectors (q), the profiles of

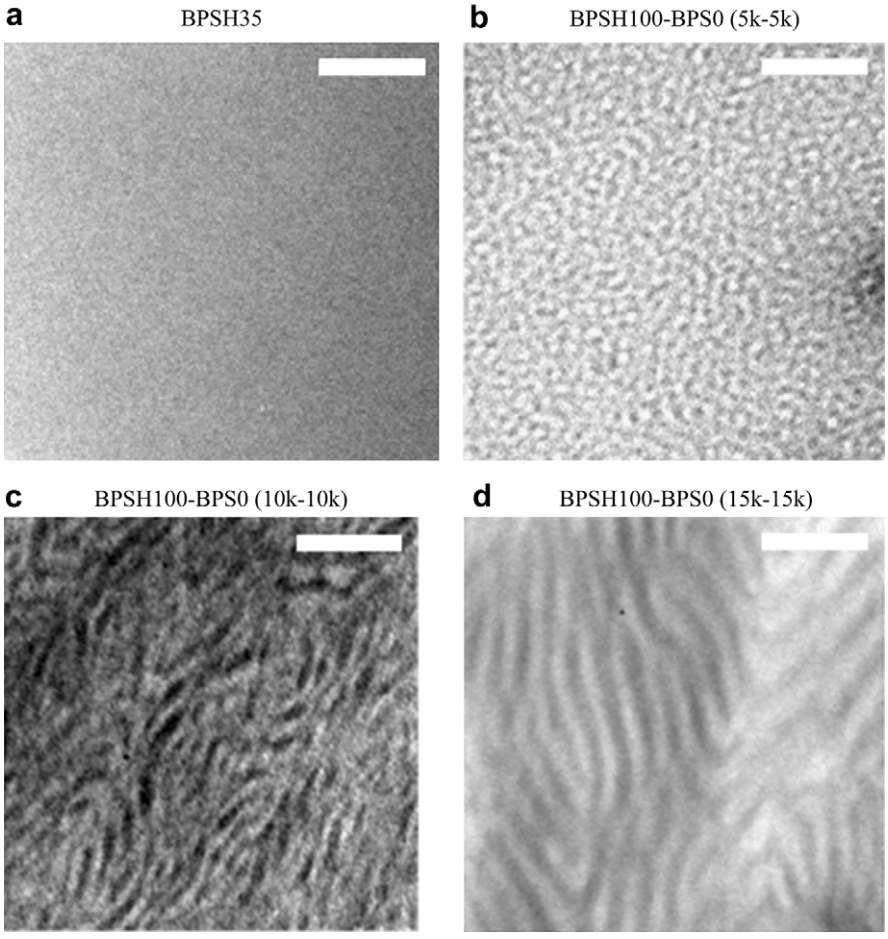

Fig. 8. TEM micrographs of the copolymer films cast with NMP and dried at 20 °C. Length of scale bar = 100 nm.

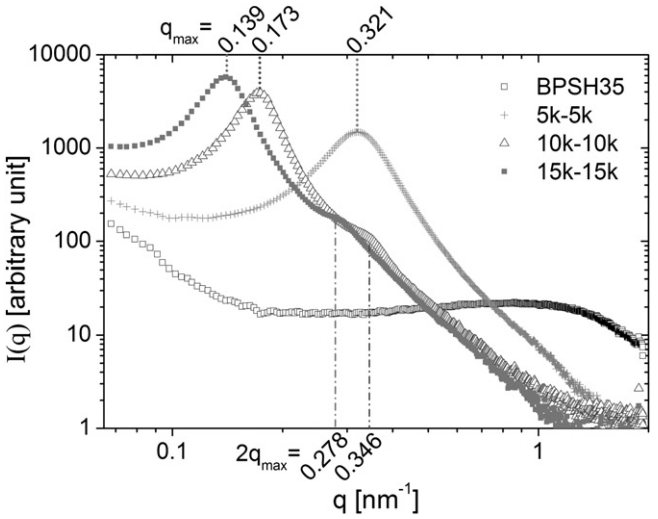

Fig. 9. SAXS profiles of the BPSH100–BPS0 multiblock copolymer films cast with NMP and dried at 20 °C.

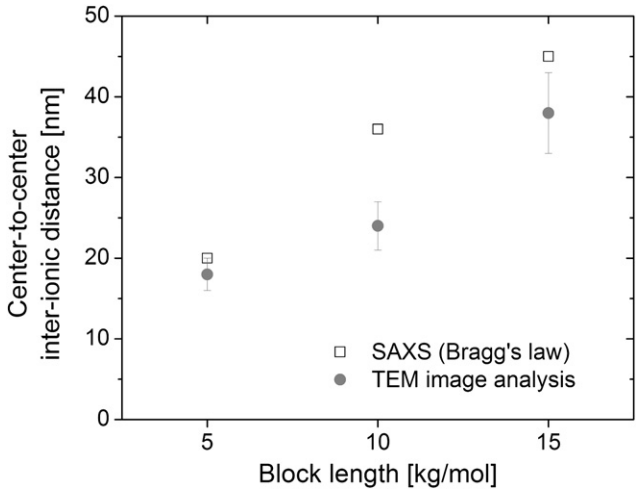

Fig. 10. Comparison of the distance between the ionic domains estimated from the SAXS profiles and TEM images of the BPSH100–BPS0 multiblock copolymer films cast with NMP and dried at 20 °C.

each multiblock copolymer film exhibited pronounced scattering maxima, while the profile of the BPSH35 random copolymer film was essentially featureless. In agreement with the TEM results, the scattering maxima observed for the multiblock copolymers can be attributed to the nano-phase-separated ionic domains. These SAXS profiles of the multiblock copolymer films also confirm the presence of ordered periodic microstructures that are dependent on block length. For the 10 k and 15 k multiblock copolymers, two characteristic scattering features were observed, including a sharp Gaussian peak (i.e., the main scattering maximum) and a weak 2nd-order peak apparent at $2q_{max}$ (q_{max} is the scattering wave vector of the main scattering maximum). In general, highly ordered lamellar microstructures often show a series of peaks at q_{max}, $2q_{max}$, $3q_{max}$, … [34,35]. Thus, the scattering behavior observed for the 10 k and 15 k multiblock copolymers confirms the presence of a well-ordered lamellar morphology [36], again consistent with the TEM data in Fig. 8. For the 5 k multiblock copolymer, however, only one broad maximum was observed. This scattering behavior suggests that the short block lengths, while clearly phase-separated, inhibit the formation of well-defined lamella with long-range periodicity. Therefore, the multiblock copolymers consisting of longer blocks are found to develop a more ordered and long-range periodic structure.

As the block length is increased, the main scattering peak is observed to shift systematically to lower q values (becoming stronger and sharper), which indicates an increase in the inter-domain spacing. The position of the SAXS maxima may be used to estimate the center-to-center distance, d_{Bragg}, between the ionic domains using Bragg's law, where $d_{Bragg} = 2\pi/q_{max}$. The estimated values of the inter-ionic-domain distance using Bragg's law are plotted in Fig. 10 with a comparison to measured values obtained by analyzing the TEM micrographs (Fig. 8(b)∼(d)). The TEM micrograph analysis was conducted by manually measuring the distances between centers of two parallel ionic domains. Given the fact that SAXS and TEM provide measurements of global vs. local dimensions, respectively, the qualitative agreement between these two techniques is significant.

The effects of solvent selectivity and drying temperature on the final microstructures were also investigated using TEM and SAXS. The scattering profiles of the 10 k and 15 k films cast with NMP and DMAC are compared in Fig. 11. The films cast from DMAC and NMP showed similar scattering profiles, e.g., Gaussian peaks and 2nd-order shoulders located at $2q_{max}$, indicating of the formation of periodically ordered lamellar structures. However, the DMAC films exhibited stronger 2nd-order peaks, compared with the NMP films. This scattering behavior indicates that the DMAC film-casting process yields a more ordered lamellar structure with longer-range periodicity [37]. This enhanced, long-range order may be attributed to the selective nature of DMAC (as described in Section 3.2), relative to NMP ($\chi_{BPS0-DMAC} > \chi_{BPS0-NMP}$), which allows for higher water uptake and proton conductivity, as shown in Figs. 4 and 5.

The effects of drying temperature on the resulting morphology can be observed from the comparison of TEM micrographs in Fig. 12. The 15 k NMP film dried at 20 °C and 80 °C showed a phase-separated microstructure with similar inter-domain dimensions; however, the film dried at 20 °C showed more refined lamella having wider lateral dimensions (i.e., longer-range domain continuity). This effect of drying temperature can be explained by two possible reasons: reduced incompatibility and/or shortened total drying time at higher temperatures. First, changes in the thermodynamic compatibility between the chemical species within the polymer solution could significantly affect the resulting microstructures of

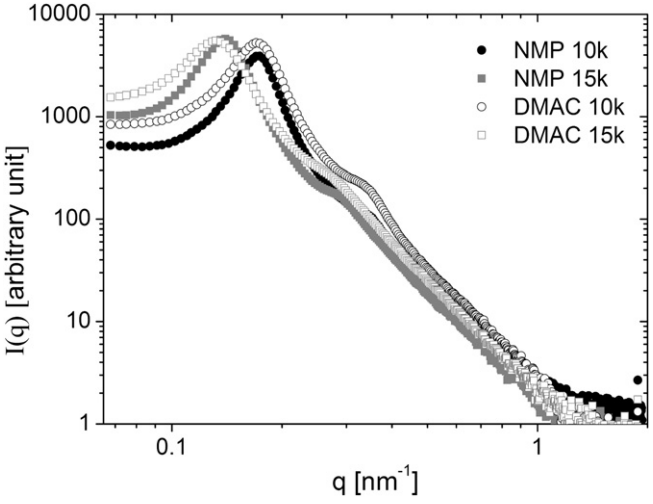

Fig. 11. Comparison of the SAXS profiles of the BPSH100–BPS0 multiblock copolymer films cast with NMP and DMAC and dried at 20 °C.

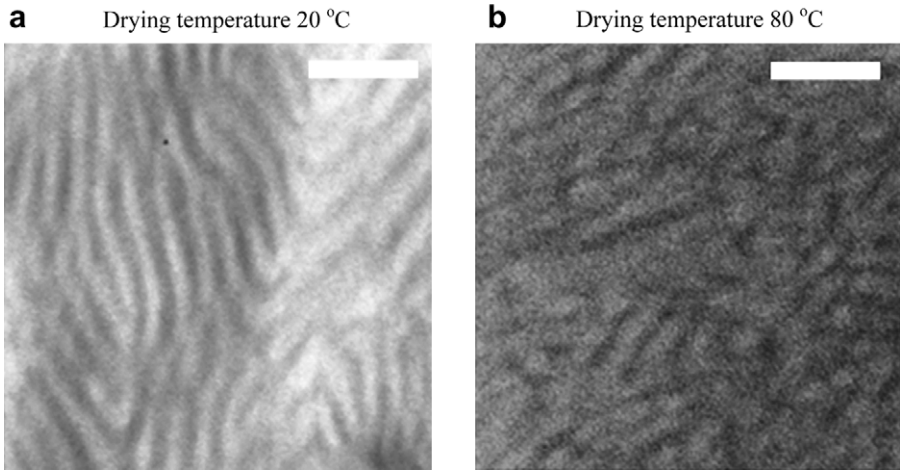

Fig. 12. TEM micrographs of the BPSH100–BPS0 (15–15 k) multiblock copolymer films cast with NMP and dried at (a) 20 and (b) 80 °C. Length of scale bar = 100 nm.

the multiblock copolymers. The interaction parameter, which represents a measure of the thermodynamic interactions between two chemical species, is inversely proportional to temperature (i.e., $\chi_{AB} = C_1 + C_2/T$). As the temperature increases, the magnitude of the interaction parameter decreases (to lower positive values) reflecting an increase in compatibility between the interacting species (i.e., a reduction in the thermodynamic driving force for phase separation). Thus, the increased compatibility at higher temperatures might weaken the phase separation between the sulfonated and unsulfonated blocks.

The second possible reason for the effect of drying conditions on the resulting morphology involves the kinetics of phase separation. As previously described, the total drying time depends significantly on the temperature of the convection air. As shown in Fig. 3, drying at two different temperatures, 20 and 80 °C, led to a profound difference in the total drying time, by more than an order of magnitude. With very rapid drying (i.e., at 80 °C), the time required to achieve complete morphological development might exceed the drying time. Because molecular mobility in these multiblock copolymers is facilitated by the presence of solvent, rapid solvent evaporation might result in a morphology that is kinetically-trapped as the chains become immobilized in the solvent-free state. As shown in Fig. 12, the film dried at 20 °C had a well-defined microstructure with more continuous and larger ionic domains, so its water uptake was higher than that of the film dried at 80 °C. Since the excessive swelling of the 20 °C films led to a reduction in the volume-based IEC_v values, the proton conductivity is virtually independent of drying temperature, as previously discussed. This behavior suggests that the drying temperature is a useful processing parameter for tailoring membrane properties. Specifically, these data show that water uptake can be minimized without sacrificing high proton conductivity, which is quite desirable for PEM applications.

4. Conclusions

The effects of block length and solution-casting conditions on the final microstructures and properties of disulfonated poly (arylene ether sulfone) multiblock copolymer (BPSH100–BPS0) films for PEMs were investigated based on the basic principles of microstructure formation of block copolymers. Morphological studies with TEM and SAXS demonstrated that the multiblock architectures could yield ordered lamellar morphologies having long-range continuity and periodicity. In contrast, random copolymers of a comparable ionic content (i.e., BPSH35) did not show evidence of distinct ionic domains, due to a more homogeneous distribution of charged units throughout the ionomer matrix.

Morphological development within the multiblock ionomers was also found to be dependent on the block length. With an increase in block length, the inter-ionic-domain distance increased, with a subsequent increase in lamellar ordering and long-range continuity. This enhancement in lamellar order with increasing block length resulted in higher water uptake and proton conductivity. Further enhancements in morphological order were observed through utilization of a selective solvent, DMAC, which provided a considerable increase in both water uptake and proton conductivity.

Film drying temperature also turned out to be an important processing parameter for tailoring the performance of these multiblock ionomers as PEMs. Drying of the multiblock copolymer films at lower temperatures facilitated morphological development and enabled higher water uptake, especially for the DMAC films. However, the high proton conductivity observed for the well-order multiblock systems was found to be rather independent of drying temperature. The drying temperature effects were ascribed to the temperature-dependence of the incompatibility between chemical species and/or to the kinetics of phase separation within the multiblock copolymers. The abovementioned effects were more obvious as the block length increased, implying that the multiblock copolymer consisting of longer blocks were more responsive to the variations of casting conditions.

For the series of copolymers studied here, the morphology-property results suggest that the block length should be above ca. 10 kg/mol to noticeably improve the morphological order, and enhance the proton conductivity of the BPSH100–BPS0 multiblock copolymer films for potential PEM applications. It is also important to note that casting of the BPSH100–BPS0 multiblock copolymers with a selective solvent, DMAC, followed by film drying at a higher temperature, could lead to the development of PEM with improved proton conductivity and controlled water uptake.

Acknowledgement

The authors wish to thank the U.S. Department of Energy (DOE) for their support of this study (Grant No. DE-FG36-06G016038). Use of the National Synchrotron Light Source, Brookhaven National laboratory, was also supported by the DOE (Grant No. DE-AC02-98CH10886) and the NSF (Grant No. CMMI-0707364 and CBET-0756439).

References

[1] Devanathan R. Energy & Environmental Science 2008;1:101.
[2] Sopian K, Wan Daud WR. Renewable Energy 2006;31:719.
[3] Roziére J, Jones DJ. Annual Review of Materials Research 2003;33:503.
[4] Costamagna P, Srinivasan S. Journal of Power Sources 2001;102:242.
[5] Hickner MA, Ghassemi H, Kim YS, Einsla BR, McGrath JE. Chemical Reviews 2004;104:4587.
[6] Vishnyakov VM. Vacuum 2006;80:1053.
[7] Kim YS, Dong L, Hickner MA, Glass TE, Webb V, McGrath JE. Macromolecules 2003;36:6281.
[8] Savadogo O. Journal of Power Sources 2004;127:135.
[9] Thampan TM, Jalani NH, Choi P, Datta R. Journal of the Electrochemical Society 2005;152:A316.
[10] Kreuer KD. Journal of Membrane Science 2001;185:29.
[11] Lee HS, Roy A, Lane O, Dunn S, McGrath JE. Polymer 2008;49:715.
[12] Lee HS, Roy A, Lane O, McGrath JE. Polymer 2008;49:5387.
[13] Lee HS, Badami A, Roy A, McGrath JE. Journal of Polymer Science, Part B: Polymer Physics 2007;45:4879.
[14] Zhao C, Lin H, Shao K, Le X, Ni H, Wang Z, et al. Journal of Power Sources 2006;162:1003.
[15] Wang H, Badami A, Roy A, McGrath JE. Journal of Polymer Science, Part A: Polymer Chemistry 2006;45:284.
[16] Ghassemi H, Ndip G, McGrath JE. Polymer 2004;45:5855.
[17] Hamley IW. The physics of block copolymers. Oxford; New York: Oxford University Press; 1998.
[18] Gutoff EB, Cohen ED. Coating and drying defects – troubleshooting operating problems. New York: John Wiley & Sons, Inc.; 1995.
[19] Bébin P, Galiano H. Advances in Polymer Technology 2006;25:121.
[20] Bébin P, Galiano H. Advances in Polymer Technology 2006;25:127.
[21] Robertson GP, Mikhailenko SD, Wang K, Xing P, Guiver MD, Kaliaguine S. Journal of Membrane Science 2003;219:113.
[22] Huang J, Baird DG, Fan G, Zhang Z, Badami A, Takamuku S, et al. 2007 Society of Plastics Engineers Annual Conference, Cincinnati, OH; 2007.
[23] Khandpur AK, Förster S, Bates FS, Hamley IW, Ryan AJ, Bras W, et al. Macromolecules 1995;28:8796.
[24] Hamley IW. Introduction to block copolymers. In: Hamley IW, editor. Developments in block copolymer science and technology. John Wiley & Sons, Ltd; 2004.
[25] Hanley KJ, Lodge TP, Huang CI. Macromolecules 2000;33:5918.
[26] Huang H, Zhang F, Hu Z, Du B, He T, Lee FK, et al. Macromolecules 2003;36:4084.
[27] Wang F, Hickner M, Kim YS, Zawodzinski TA, McGrath JE. Journal of Membrane Science 2002;197:231.
[28] Cohen ED, Gutoff EB. Modern coating and drying technology. New York: Wiley-VCH; 1992.
[29] Romdhane IH, Price Jr PE, Miller CA, Benson PT, Wang S. Industrial and Engineering Chemistry Research 2001;40:3065.
[30] Zawodzinski TA, Neeman M, Sillerud LO, Gottesfeld S. Journal of Physical Chemistry 1991;95:6040.
[31] Smallwood IM. Handbook of organic solvent properties. New York: Halsted Press; 1996.
[32] Kim YS, Wang F, Hickner M, McCartney S, Hong YT, Harrison W, et al. Journal of Polymer Science, Part B: Polymer Physics 2003;41:2816.
[33] Gebel G. Polymer 2000;41:5829.
[34] Ivanova R, Lindman B, Alexandridis P. Langmuir 2000;16:3660.
[35] Th Forthwith, Fritz G, Freiberger N, Glatter O. Journal of Applied Crystallography 2004;37:703.
[36] Corvazier L, Messé L, Salou CLO, Young RN, Faircough JPA, Ryan AJ. Journal of Materials Chemistry 2001;11:2864.
[37] Young W-S, Brigandi PJ, Epps III TH. Macromolecules 2008;41:6276.